MASTCAM-Z INVESTIGATION OF THE BOULDER (BLOCKY) UNIT OF THE WESTERN FAN TOP AT JEZERO CRATER, MARS. A. Vaughan[1], B.H. Horgan[2], O. Ciancolo[3], L. Kah[3], S.J. Gwizd[4], A. Klidaras[2], N. Randazzo[5], B. Kathir[6], J.R. Johnson[7], L. Mandon[8], J. Bell III[9], A.J. Brown[10], [1]Apogee Engineering, LLC, Flagstaff, AZ, [2]Purdue University, [3]University of Tennessee, [4]Jet Propulsion Laboratory, [5]University of Alberta, [6]Western Washington University, [7]Johns Hopkins University Applied Physics Laboratory, [8]California Institute of Technology, [9]Arizona State University, [10]Plancius Research.

Introduction: The Mastcam-Z multispectral imaging system on the Perseverance rover was used to assess the diversity of boulder fields on top of the western fan in Jezero crater. These boulders are associated with what has been mapped as the "blocky unit" [1]. Understanding their relationship to the underlying sedimentary layers that compose the fan, their possible representation of material from the Jezero watershed, and their depositional history is critical to constraining past aqueous environments and fan formation/preservation. Current hypotheses regarding the emplacement of these boulders include an erosional lag of an overlying unit (such as a lava flow) or flood deposits from the Jezero watershed that represent the last episodes of water flow into the crater [2, 3]. Sampling a representative boulder would help address whether it represents material sourced from the Noachian terrain beyond Jezero crater that Perseverance may not encounter during its mission, and would also be used for cosmogenic exposure dating, to constrain the cessation of aqueous activity involved in formation of the western fan in Jezero crater.

Methods: Mastcam-Z is a pair of zoomable, stereoscopic cameras that sits atop the remote sensing mast and use of Bayer RGB filters plus 14 narrowband filters allows multispectral imaging between 442 nm and 1022 nm [4, 5]. This region is particularly useful in detecting spectral features associated with iron and discriminating between ferric compositions associated with alteration and oxidation from ferrous iron present in primary igneous minerals [4].

Two Boulder Classes. Using Mastcam-Z multispectral data, we identified two main classes of boulders along the traverse associated with the blocky unit: olivine-bearing and pyroxene-bearing. The right-eye decorrelation stretch (DCS) images made using filters centered at 1022 nm (R6), 910 nm (R3), and 800 nm (R1), have proven effective in discriminating between these two classes, and can be used to survey a landscape quickly before extracting spectra from specific targets for more detailed analysis. In these right-eye DCS images, the olivine-bearing boulders typically appear bluer in color, the pyroxene-bearing material appears purple/magenta, and dusty/regolith covered surfaces appear beige (Fig. 1), although the image-dependent nature of DCS products makes comparisons among scenes qualitative.

Results: Discriminating boulders with DCS images in this fashion across the traverse has allowed further study of their population distributions, textural, and spectral characteristics. The Fan Top Campaign (sols ~700-900) crossed distinct lobes of the western fan mapped by [6] as units i, k, m, and h. The olivine-bearing boulders are more prevalent across all lobes observed and are generally smoother, more rounded and abraded by wind-driven sand than the less populous and rougher textured pyroxene-bearing boulders. These differences in distribution and texture suggest changes in provenance of the boulders capping the various lobes of the western Jezero fan. Population statistics for these two classes of boulders and associated interpretations have been investigated by [7].

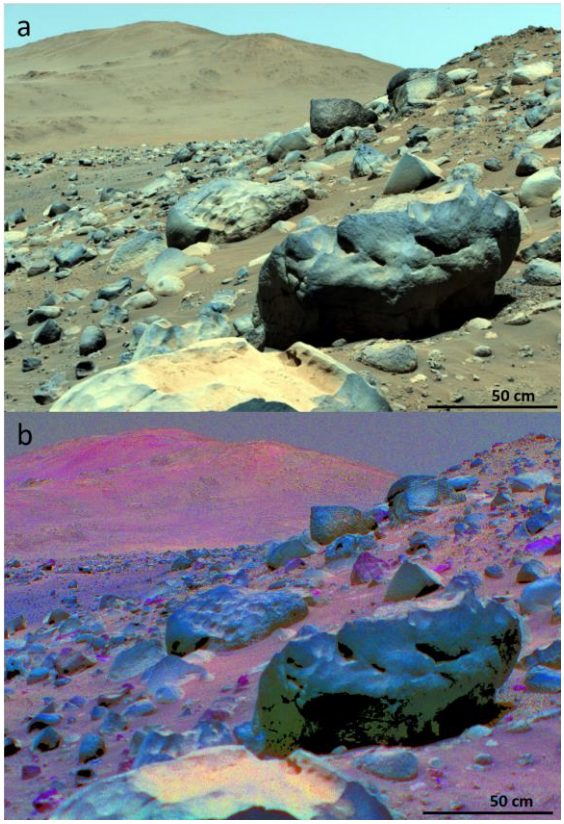

Figure 1. Sol 812 (zcam03671) Mastcam-Z R0 (enhanced Bayer filter color) of Bluebird Lake boulder field (a) and R631 DCS (b). See text for details.

Spectral Endmembers. Differences in near-infrared (NIR) spectral shape (between 800 nm and 1000 nm) enables discrimination between olivine- and pyroxene-bearing materials. The olivine class of boulders is characterized by an overall negative NIR slope con-

sistent with the1000 nm ferrous iron band present in olivine. The pyroxene class of boulders is defined by a ~900 nm absorption characteristic of ferrous iron in low-calcium pyroxenes (LCP, e.g. pigeonite, ferrosilite) (Fig. 2). In the abrasion patches, where the weathered surface is removed, there is little to no spectral evidence for ferric-iron at the diagnostic 528 nm or 866 nm wavelengths, which further supports the primary igneous mineral determinations of olivine and LCP. Weathered/natural surfaces show more oxidized spectral features consistent with dust cover and possible coatings.

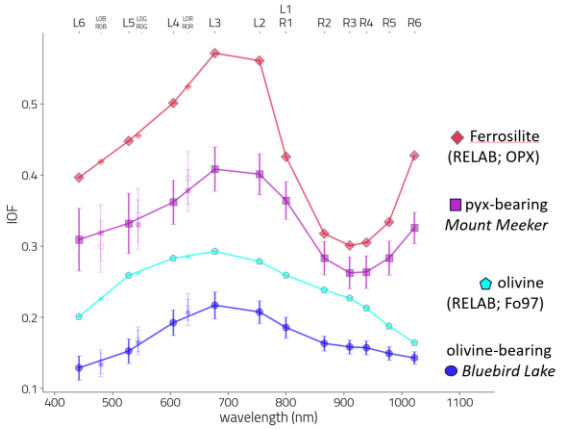

Figure 2. Mastcam-Z spectral endmembers for the olivine-bearing (blue) and pyroxene-bearing (purple) boulder classification alongside laboratory spectra (RELAB) convolved to Mastcam-Z bandpasses.

Although not yet sampled, both classes of boulders were abraded and studied by the full suite of instruments onboard Perseverance during the Fan Top Campaign, including Mastcam-Z multispectral imaging of the abraded surfaces (Fig. 3). These targets are *Lake Haiyaha* on the olivine-bearing Falcon Lake boulder, and *Dragon's Egg* on the pyroxene-bearing Mount Meeker boulder, both located on lobe i of the fan [6]. PIXL instrument data from these abrasion patches confirms the olivine- and pyroxene-dominated compositions of these two respective boulders [8, 9]. An attempt to sample the pyroxene-bearing Mount Meeker boulder was unsuccessful due to the extreme hardness of the rock and lack of drill progress.

Using a multispectral database investigation tool developed for Mastcam-Z by [11], float material across the fan top was evaluated to assess the overall diversity of the boulders and how they compare to other units investigated by Perseverance. NIR spectral parameters that effectively separate the olivine-like and LCP-like spectra allows for identification of spectral endmembers for these two classes of boulders. These parameters show that while the olivine-bearing boulders have spectral features similar to other olivine-bearing bedrock units observed in Jezero crater (e.g. the olivine-cumulate Séítah formation and the curvilinear unit), the LCP spectral features observed in the pyroxene-bearing boulders are distinctive. However, both SuperCam LIBS and PIXL data show the olivine-bearing boulders to be relatively homogenous and compositionally distinct from the Séítah olivine-cumulate formation, with enriched Mg and less alteration [8,11].

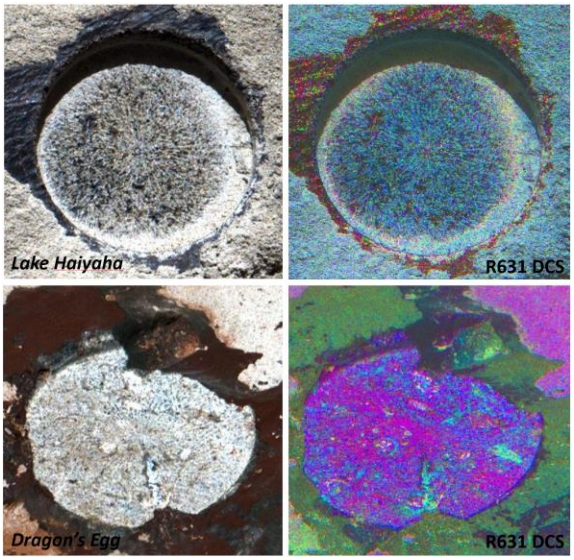

Figure 3. Mastcam-Z L0 (Bayer filter enhanced color) and R631 decorrelation stretches of the *Lake Haiyaha* (top, sol 851 zcam03700) and *Dragon's Egg* (bottom, sol 860 zcam03712) abrasion patches, each 5 cm in diameter.

Jezero Watershed: Orbital mapping [12,13,14] has shown the Jezero watershed to contain a diversity of units and compositions, including the regional olivine-carbonate unit more proximal to Jezero crater and an LCP-bearing unit more distal. The Jezero crater rim is another possible source for the boulders, as both the regional olivine unit and the LCP-bearing mafic capping unit are present in the rim. Thus, the boulder compositions are consistent with emplacement by flood deposits.

References: [1] Stack, K.M., et al. (2020) *SSR*, *216*,127. [2] Mangold, N., et. al. (2021) *Science*, *374*, 6568. [3] Gwizd, S., et al. (2024), *LPSC*, *this meeting*. [4] Bell III, J.F, et al. (2021) *SSR*, *217*,24. [5] Hayes, A.G., et al. (2021) *SSR*, *217*,29. [6] Kronyak, R.E., et. al. (2023) *LPSC LIV*, Abstract #2806. [7] Ciancolo, O.A., et al., (2024) *LPSC, this meeting.* [8] Moreland, E., et al. (2024) *LPSC, this meeting*. [9] Tremain, A. et. al., (2024) *LPSC, this meeting*. [10] Million, C. et al., (2022) *LPSC LIIV*, Abstract #2533. [11] Beyssac, O., et. al. (2024) *LPSC, this meeting*. [12] Goudge, T.A., et.al. (2015) *JGR,120*,4. [13] Mandon, L. et. al., (2020) *Icarus*, *336*,113436. [14] Scheller, E.L. and Ehlmann, B.L. (2020) *JGR,125*, 7.